Rheology of lubricant basestocks: A molecular dynamics study of C 30 isomers

J. D. Moore, S. T. Cui, H. D. Cochran, and P. T. Cummings

Citation: The Journal of Chemical Physics **113**, 8833 (2000); doi: 10.1063/1.1318768
View online: http://dx.doi.org/10.1063/1.1318768
View Table of Contents: http://scitation.aip.org/content/aip/journal/jcp/113/19?ver=pdfcov
Published by the AIP Publishing

Rheology of lubricant basestocks: A molecular dynamics study of C_{30} isomers

J. D. Moore[a] and S. T. Cui
Department of Chemical Engineering, University of Tennessee, Knoxville, Tennessee 37996 and Chemical Technology Division, Oak Ridge National Laboratory, Oak Ridge, Tennessee 37831

H. D. Cochran
Chemical Technology Division, Oak Ridge National Laboratory, Oak Ridge, Tennessee 37831 and Department of Chemical Engineering, University of Tennessee, Knoxville, Tennessee 37996

P. T. Cummings[b]
Departments of Chemical Engineering, Chemistry, and Computer Science, University of Tennessee, Knoxville, Tennessee 37996 and Chemical Technology Division, Oak Ridge National Laboratory, Oak Ridge, Tennessee 37831

(Received 5 May 2000; accepted 23 August 2000)

We have performed extensive equilibrium and nonequilibrium molecular dynamics (EMD and NEMD) simulations of three isomers of $C_{30}H_{62}$ at temperatures of 311 and 372 K employing a united atom model. Using the rotational relaxation time calculated from the EMD simulation, the Rouse model predicts a zero-shear viscosity for *n*-triacontane within 16% of the value determined by NEMD. Compared to experiment, NEMD and the united atom model underpredict the kinematic viscosities of *n*-triacontane and 9-*n*-octyldocosane but accurately predict the values for squalane (within 15%). In addition, the predicted values of the kinematic viscosity index for both 9-*n*-octyldocosane and squalane are in quantitative agreement with experiment and represent the first such predictions by molecular simulation. This same general potential model and computational approach can be used to predict this important lubricant property for potential lubricants prior to their synthesis, offering the possibility of simulation-guided lubricant design. © *2000 American Institute of Physics.* [S0021-9606(00)50643-6]

I. INTRODUCTION

An understanding of the relationship between chemical structure and lubricant performance is highly desirable from both a fundamental and a practical perspective. From the standpoint of fundamental science, making the connection between microscopic and macroscopic properties is always an area of keen interest. In practical terms, such knowledge is crucial both to improve the performance of mineral oils and to guide the design of synthetic lubricants, driven by both long-term and contemporary motivations. Though they still make up less than 5% of the total lubricant market, demand for synthetics is increasing for many present-day applications because they provide greater stability and reliability, leading to less wear on machinery and longer intervals between oil changes.[1] In addition, advances in automotive engine design to ensure improved efficiency and reduced emissions are expected to make severe demands on lubricants in the form of higher operating temperatures and, perhaps, higher strain rates, demands which most lubricants currently on the market will be unable to meet.

Since alkanes of intermediate molecular size ($C_{20}H_{42}$–$C_{40}H_{82}$) are the main constituents of lubricant basestocks, their rheological properties are of great concern in industrial lubricant applications. Certain general trends in the structure–property relationships of these molecules are well known. For example, though the viscosities of the straight chain paraffins vary little with temperature (a basic characteristic of a good lubricant), they are solids at room temperature. For this reason, most of the linear alkanes are removed from base oils during refining to improve their low-temperature performance. Much of what is known about the structure–property relationships of alkanes is based on API Research Project 42, a database containing physical properties of 273 pure hydrocarbons.[2] Among other properties, it contains viscosity measurements at a variety of temperatures for most of the 273 compounds. Since viscosity index, flash point, and pour point, in addition to viscosity, are the most important properties of a lubricant,[3] Denis analyzed the data in API 42 in an attempt to identify which molecular structures tend to provide the best compromise between the desirable properties of high viscosity index (minimal variation of viscosity with temperature) and low pour point.[4] Though the amount of data contained in API 42 is certainly extensive, it by no means provides a complete picture. In fact, of the greater than four billion possible alkanes containing 30 total carbons, only 2 are represented in API 42. Hence, there appears to be insufficient data to predict how the details of molecular structure will affect lubricant properties short of additional synthesis, formulation, and testing. Such a process is expensive and time-consuming.

[a]Current address: The Dow Chemical Company, Midland, Michigan 48674.
[b]Author to whom correspondence should be addressed; electronic mail: ptc@utk.edu

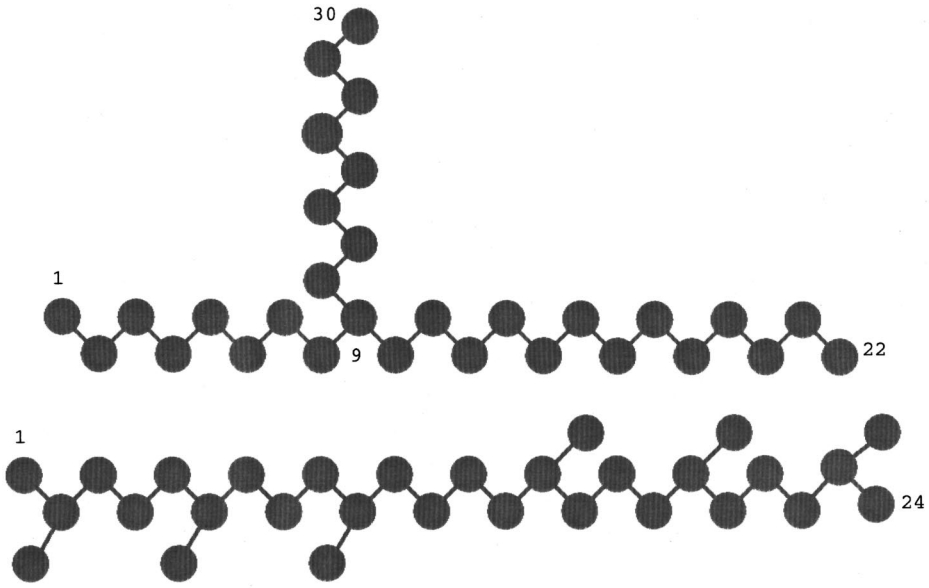

FIG. 1. Cartoons of the branched alkanes included in this study. (a) 9-*n*-octyldocosane and (b) squalane.

Molecular simulation is emerging as an ideal alternative. Given an accurate transferable intermolecular potential model and a working simulation code of sufficient generality, the modification of only a few lines of code is necessary for the virtual synthesis of alkanes exhibiting any of the possible molecular architectures. Though realistic study of the relevant systems ($C_{20}H_{42}$–$C_{40}H_{82}$) by molecular simulation has previously been limited by both high computational costs and the lack of potential models accurate over a wide range of physical conditions, advances in models[5] and algorithms[6] as well as the advent of massively parallel supercomputers have now made such studies possible. In addition, the severe conditions commonly found in engines and other machinery (film thickness$<1\ \mu$m, $\dot{\gamma}>10^7\ s^{-1}$, $P\simeq 10^9$ Pa[7,8]) are extremely difficult to study experimentally and yet are quite readily accessible to simulation, nonequilibrium molecular dynamics (NEMD)[9,10] in particular. So far, only a few studies have used NEMD to investigate the effect of branching on the rheology of alkanes of intermediate size.[11–16]

Utilizing a united atom model for alkanes[5,17] and rRESPA multi-time-step dynamics[6,18,19] incorporating a Nosé thermostat, we present the results of equilibrium (EMD) and nonequilibrium molecular dynamics simulations of three isomers of $C_{30}H_{62}$: *n*-triacontane, 9-*n*-octyldocosane, and squalane (the architectures of the branched molecules are illustrated in Fig. 1). The potential model used for the linear and branched alkanes is essentially the same as the united atom model for alkanes proposed by Siepmann *et al.*[5] (SKS) for linear alkanes and extended to branched alkanes by Mondello and Grest,[17] with the modification that the fixed bond length is replaced by a stiff harmonic bond-stretching potential. All of the intramolecular interactions were treated as fast motions (smaller time step of 0.47 fs) and the intermolecular interaction as the slow motion (larger time step of 2.35 fs). The EMD simulations focus primarily on calculations of the self-diffusion coefficients and rotational relaxation times for triacontane (372 K) and octyldocosane (311 and 372 K), including comparison to results for squalane reported by Mondello and Grest.[17] The NEMD simulations reveal the dependence of a variety of properties on strain rate for *n*-triacontane (372 K), squalane (311 and 372 K), and 9-*n*-octyldocosane (311 and 372 K). Simulations were not performed for triacontane at 311 K because experimentally it is a solid at that temperature. As was reported previously for squalane,[13] the kinematic viscosity index of 9-*n*-octyldocosane calculated based on our simulations is found to be in excellent agreement with the experimental value.

II. RESULTS AND DISCUSSION

The constant-*NVT* simulations involved 100 $C_{30}H_{62}$ molecules (i.e., 3000 united atoms) at temperatures of 311 and 372 K and the corresponding experimental densities at 0.1 MPa pressure[2] (see Table I). The density for *n*-triacontane at 372 K was estimated by interpolation between *n*-octadocosane and *n*-dotriacontane. Subsequent to equilibration, we accumulated the equilibrium properties of the systems as well as the nonequilibrium properties at shear rates ranging from 2.1×10^8 to $4.3\times10^{11}\ s^{-1}$ (i.e., reduced shear rates $\dot{\gamma}(m\sigma^2/\epsilon)^{1/2}$ 0.0005 to 1.0 at which we do not expect the results to depend significantly on the details of the thermostat.[20,21]).

A. Equilibrium translational and rotational diffusion

Though our primary interests lie in the area of rheology, several equilibrium properties are of interest as well, including the self-diffusion coefficient and rotational relaxation

TABLE I. State points simulated.

Molecule	T (K)	ρ (g/cm^3)
n-triacontane	372	0.7596
9-*n*-octyldocosane	311	0.7999
	372	0.7609
squalane	311	0.7979
	372	0.7592

TABLE II. Equilibrium properties.

	311 K			372 K		
Molecule	P (MPa)	R_g^2 (Å^2)	% Trans	P (MPa)	R_g^2 (Å^2)	% Trans
n-triacontane	⋯	⋯	⋯	31.6(3)	65.6(2)	69.5(1)
9-*n*-octyldocosane	30.0(6)	44.3(1)	67.9(1)	29.9(2)	43.1(1)	65.0(1)
squalane[a]	−66.2(6)	49.0(5)	⋯	−55.0(3)	46.0(3)	⋯

[a]Data from Ref. 17.

time. In particular, the rotational relaxation time is important because it aids in analyzing viscosity versus strain-rate data in terms of the critical strain rate for transition from Newtonian to non-Newtonian behavior.[15,22] Also, both properties can be used in conjunction with results from the Rouse model[23] of unentangled polymer melts to predict the zero-shear viscosity for linear chains.[24] The average hydrostatic pressure (trace of the pressure tensor with no long-range corrections), squared radius of gyration, and percentage *trans* bonds data calculated by EMD are given in Table II (the numbers in parentheses represent the statistical uncertainty in the least significant digits). These values are averaged over runs of 4.0 ns for 9-*n*-octyldocosane at both temperatures and 3.3 ns for *n*-triacontane.

The self-diffusion coefficients of the alkane melts are estimated from EMD simulations in terms of the limiting slope of the mean squared displacement (MSD) of the chain centers of mass as a function of time based on the Einstein relation

$$2tD=\frac{1}{3}\langle|r_i(t)-r_i(0)|^2\rangle, \tag{1}$$

where D is the self-diffusion coefficient and r_i is the position of the center of mass of molecule i. The notation $\langle ... \rangle$ is indicative of the fact that the MSD was averaged over the 100 molecules in each system as well as 1980, 7045, and 5550 different time origins and corresponding initial positions $r_i(0)$ for the 9-*n*-octyldocosane at 311 K, 9-*n*-octyldocosane at 372 K, and *n*-triacontane at 372 K runs, respectively. Each time origin was separated from the previous one by 1.175 ps at 311 K and 0.47 ps at 372 K. The diffusion results (including results for squalane reported by Mondello and Grest[17]) are given in Table III. The model overpredicts the experimental self-diffusion coefficients for squalane by approximately 30% at these two temperatures.[17]

TABLE III. Equilibrium results: Translational and rotational diffusion.

	311 K			372 K		
Molecule	D (10^{-6} cm^2/s)	τ_1 (ns)	τ_2 (ns)	D (10^{-6} cm^2/s)	τ_1 (ns)	τ_2 (ns)
n-triacontane	⋯	⋯	⋯	5.92 [3.68][a]	0.44	0.21
9-*n*-octyldocosane	0.89	0.68	0.64	3.70	0.25	0.18
squalane[c]	0.62 [0.48][b]	2.85	2.24	3.39 [2.60][b]	0.46	0.19

[a]Number in brackets is the experimental value interpolated from data in Ref. 25.
[b]Number of brackets is the experimental value from Ref. 17.
[c]Reference 17.

The value predicted for *n*-triacontane is approximately 60% larger than the experimental one.[25] Such overprediction of the self-diffusion coefficient is typical of the SKS united atom model. Better agreement with experiment for linear chains has been achieved[17,24] by either introducing a displacement between the centers of force of nonbonded interactions and the centers of mass of the united atoms (the so-called ''anisotropic united atom'' model)[26,27] or by using a different torsional parameterization and slightly larger Lennard-Jones (LJ) size parameter.[28] The authors have been unable to find experimental data for the diffusivity of 9-*n*-octyldocosane. We have attempted to analyze the global rotational motion of the molecules as characterized by the orientational relaxation of the longest principal axis (e_1) of each molecule's ellipsoid of inertia. We measure the first- and second-order angular correlation functions

$$P_1^{e_1}(t)=\langle e_1(t)\cdot e_1(0)\rangle \tag{2}$$

and

$$P_2^{e_1}(t)=\frac{1}{2}(3\langle[e_1(t)\cdot e_1(0)]^2\rangle-1). \tag{3}$$

Ignoring the short-time behavior, the functions exhibit exponential decay with characteristic relaxation times τ_1 and τ_2. The same numbers and frequencies of time origins that were used for the translational diffusion calculations were also used for the rotational relaxation time calculations. The results for the various molecules are given in Table III. For isotropic rotational diffusion, $\tau_1/\tau_2=3$ is expected.[29,30] For each case given in Table III, τ_1/τ_2 is significantly less than 3, indicating that the orientational relaxation of the molecules is spatially constrained.[31] $\tau_1/\tau_2\approx 2$ for squalane and *n*-triacontane at 372 K and approaches a value of 1 for squalane at 311 K and 9-*n*-octyldocosane at both temperatures. Previous NEMD studies[15,22] have demonstrated that the transition from Newtonian to shear-thinning behavior of alkane liquids of length up to C_{24} occurs at a critical strain rate ($\dot{\gamma}_c$) approximately equal to $1/\tau_1$. Thus, our EMD results suggest that the transition to non-Newtonian behavior will occur at smaller strain rates for squalane than for 9-*n*-octyldocosane at both the temperatures studied while at 372 K the transition should occur at approximately the same strain rate for squalane and *n*-triacontane.

Using results from the Rouse model, expressions for the zero-shear viscosity of a polymer melt can be written in terms of properties that can be measured during an EMD simulation. In terms of the rotational relaxation time τ_1,

$$\eta_\tau=\frac{\pi^2\rho RT\tau_1}{12M}, \tag{4}$$

where ρ is the density, T is the temperature, R is the gas constant, and M is the molecular weight. Mondello *et al.*[24,32] have compared the various estimates of the zero-shear viscosity based on the Rouse model and properties from EMD simulations to the viscosity calculated by NEMD at a strain rate less than $\dot{\gamma}_c=\tau_1^{-1}$ for alkanes ranging from $C_{10}H_{22}$ to $C_{66}H_{134}$. They found that $\eta_\tau\approx\eta_{\mathrm{NEMD}}$ (within 20%) for all of the systems studied. The estimates of the zero-shear kine-

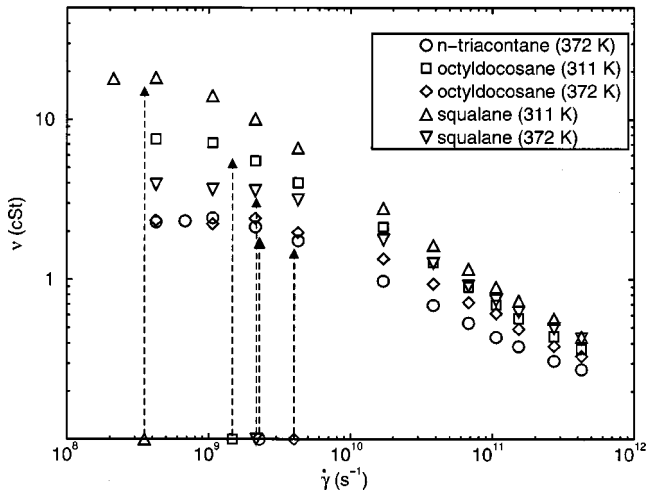

FIG. 2. Kinematic viscosity vs strain rate for *n*-triacontane, 9-*n*-octyldocosane, and squalane. The dashed lines extending from the symbols on the horizontal axis up to the filled triangles indicate τ_1^{-1} for the molecule and state corresponding to the symbol from which they extend.

matic viscosity ($\nu = \eta/\rho$) of *n*-triacontane at 372 K using the properties from our EMD simulation are $\eta_\tau = 2.66 \times 10^{-6}\,\mathrm{m^2/s}$.

B. Viscosity

Kinematic viscosity is plotted in Fig. 2 as a function of strain rate. Error bars are suppressed for clarity since they are smaller than the symbols except at certain of the lowest strain rates. In all cases, the viscosity shows shear thinning behavior over most of the range of strain rates and a Newtonian plateau at the lowest strain rates. The dashed lines extending from the symbols on the horizontal axis up to the filled triangles indicate τ_1^{-1} for the molecule and state corresponding to the symbol from which it extends. Thus, the transition from Newtonian to non-Newtonian behavior correlates well with the inverse of the rotational relaxation time. Though the Newtonian plateaus of *n*-triacontane and 9-*n*-octyldocosane are indistinguishable from each other at 372 K, their viscosities are clearly distinguishable in the shear thinning region, indicating that the transition to shear thinning occurs at a lower strain rate for *n*-triacontane than for 9-*n*-octyldocosane. This conclusion is also supported by the τ_1^{-1} data. Each viscosity value in the plateau region is considered an independent prediction of the zero-shear viscosity, and the uncertainty in the zero-shear value is estimated by considering the scatter in the plateau viscosities relative to their average. The strain rates and viscosities considered to fall within the plateau region are given in Table IV, and the corresponding predictions of the zero-shear viscosity and kinematic viscosity index (VI) are given in Table V along with the experimental values. The experimental zero-shear viscosity for *n*-triacontane was estimated by interpolation between *n*-octadocosane and *n*-dotriacontane. The kinematic viscosity index (VI) is a widely used industrial characterization of automotive lubricants. Based on the kinematic viscosity of the oil at 40 and 100 °C, the VI is an attempt to quantify an oil's viscosity-temperature behavior. The higher a lubricant's viscosity index, the less the lubricant's viscosity varies with temperature. We have calculated the VI according to the ASTM standards (ASTM D2270-93 and ASTM D341-93). The uncertainty in the VI values was estimated by propagating the uncertainty in the zero-shear viscosities (assumed to be 5% for the experimental measurements). Compared to experiment, the united atom model underpredicted the kinematic viscosities of *n*-triacontane and 9-*n*-octyldocosane but accurately predicted the values for squalane (within 15%). In addition, the VI values predicted by NEMD and the united atom model are in quantitative agreement with experiment. That is, even though the united atom model did not accurately predict the viscosities for 9-*n*-octyldocosane, it still did an excellent job of predicting the dependence of its viscosity on temperature. Also, the zero-shear viscosity for *n*-triacontane predicted from the value of τ_1 from simulation and results from the Rouse model was within 16% of the value determined by NEMD.

In Fig. 2 the ν versus $\dot{\gamma}$ curves exhibit a clear trend, though quite widely separated at low strain rate (except for *n*-triacontane in comparison to 9-*n*-octyldocosane at 372 K), to converge in the limit of high strain rate. Such a trend has been observed in simulations of alkanes[33] and experimentally for various silicone oils[34] and polystyrene solutions.[35] The power law exponents of the shear thinning region are -0.40 (*n*-triacontane, $T = 372\,\mathrm{K}$), -0.55 (9-*n*-octyldocosane, $T = 311\,\mathrm{K}$), -0.44 (9-*n*-octyldocosane,

TABLE IV. Shear rates within the Newtonian plateau.

Molecule and state	Strain rate (s^{-1})	Reduced strain rate $\dot{\gamma}(m\sigma^2/\epsilon)^{1/2}$	Kinematic viscosity ($10^{-6}\,m^2/s$)	Run length (ns)
n-triacontane	4.251×10^8	0.001	2.29(18)	21.7
372 K	6.809×10^8	0.0016	2.33(14)	14.3
	1.063×10^9	0.0025	2.44(9)	12.7
	2.126×10^9	0.005	2.14(5)	14.0
9-*n*-octyldocosane	4.251×10^8	0.001	7.53(30)	15.8
311 K	1.063×10^9	0.0025	7.16(21)	6.4
9-*n*-octyldocosane	4.251×10^8	0.001	2.35(21)	19.8
372 K	1.063×10^9	0.0025	2.23(12)	9.4
	2.126×10^9	0.005	2.42(11)	3.2
squalane	2.126×10^8	0.0005	18.1(28)	9.4
311 K	4.251×10^8	0.001	18.3(17)	7.0
squalane	4.251×10^8	0.001	3.93(48)	4.6
372 K	1.063×10^9	0.0025	3.79(46)	4.5
	2.126×10^9	0.005	3.55(13)	5.4

TABLE V. Zero-shear viscosities and VI.

Molecule and source	Kinematic viscosity ($10^{-6}\,m^2/s$) 311 K	Kinematic viscosity ($10^{-6}\,m^2/s$) 372 K	Kinematic viscosity index
n-triacontane NEMD	···	2.3±0.1	···
n-triacontane expt.[a]	···	4.4±0.2	···
9-*n*-octyldocosane NEMD	7.3±0.2	2.3±0.1	153±34
9-*n*-octyldocosane expt.[a]	14.4±0.7	3.6±0.2	143±45
squalane NEMD	18.2±0.1	3.8±0.2	103±18
squalane expt.[a]	20.9±1.0	4.2±0.2	116±30

[a]Reference 2.

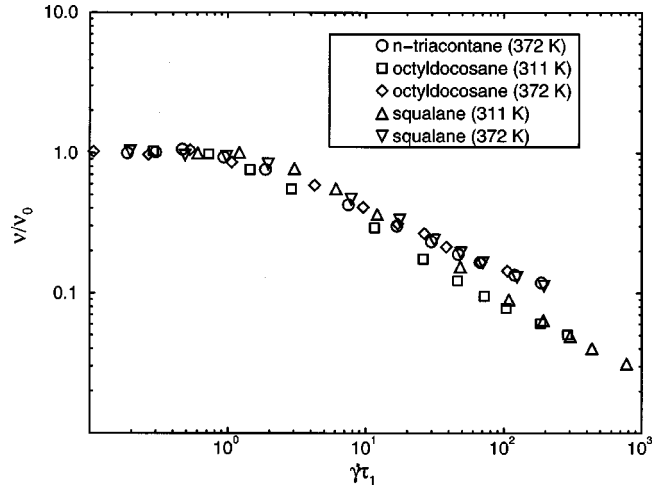

FIG. 3. Kinematic viscosity divided by zero-shear kinematic viscosity vs $\dot{\gamma}\tau_1$ for *n*-triacontane, 9-*n*-octyldocosane, and squalane.

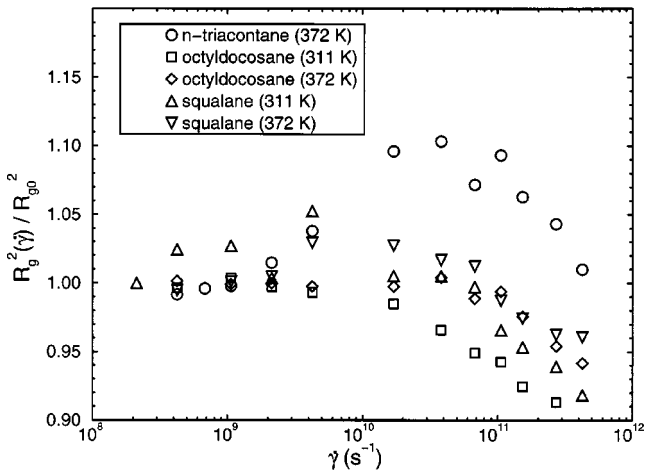

FIG. 4. Squared radius of gyration (R_g^2) divided by its value at low shear rate (R_{g0}^2) $\dot{\gamma}$ for *n*-triacontane, 9-*n*-octyldocosane, and squalane plotted as a function of strain rate.

$T=372\,\mathrm{K}$), -0.59 (squalane, $T=311\,\mathrm{K}$), and -0.45 (squalane, $T=372\,\mathrm{K}$). Since the curves tend to converge at high strain rates, the power-law exponents are necessarily larger at the lower temperature (where the zero-shear viscosities are higher). Kinematic viscosity divided by zero-shear kinematic viscosity versus $\dot{\gamma}\tau_1$ is plotted in Fig. 3. As is evident from this figure, except for values of the zero-shear viscosity and rotational relaxation time, the ν versus $\dot{\gamma}$ curves vary little with molecular architecture at a single temperature. Comparing the basic curve shapes at the two temperatures, the primary effect of decreasing temperature is to strengthen the shear thinning behavior (i.e., more negative power-law exponent).

The fact that the united atom model predicted quantitatively accurate zero-shear viscosities for squalane but significantly underpredicted those of *n*-triacontane and 9-*n*-octyldocosane (performance more typical of united atom model predictions of alkane viscosities) merits some further discussion. Allen and Rowley[36] hypothesized that the common deficiency of united atom models in predicting alkane viscosities may be due in part to their inability to model the additional drag caused by the interaction of hydrogen atoms on molecules in different velocity layers as they shear past one another; that is, in some sense, the ''smoothness'' in the united atom representation of alkanes introduced by not explicitly modeling the hydrogens leads to underprediction of alkane viscosities. We have considered the possibility that the ''knobby-ness'' of squalane's molecular architecture caused by the six methyl side-branches somehow alleviated this ''smoothness'' problem leading to quantitatively accurate viscosity predictions for squalane. However, this explanation is inconsistent with the observations of Mundy *et al.*[11] who performed simulations of squalane ($T=450\,\mathrm{K}$, $P=1$ atm) using a different extension of the SKS model to branched alkanes ($\sigma_{\mathrm{CH_3}}=\sigma_{\mathrm{CH_2}}=3.93\,\text{Å}$, $\sigma_{\mathrm{CH}}=3.85\,\text{Å}$, $\epsilon_{\mathrm{CH_3}}/k_B(\text{methyl branch})=78\,\mathrm{K}$, $\epsilon_{\mathrm{CH_2}}/k_B=47\,\mathrm{K}$, $\epsilon_{\mathrm{CH}}/k_B=32\,\mathrm{K}$).[37] At least in the limit of low strain rate, they were unable to observe a statistical difference between the viscosity of squalane and that of *n*-triacontane (simulated at the same T and P). In a note added in proof,[37] Siepmann *et al.* provided revised parameters for branched alkanes ($\sigma_{\mathrm{CH_3}}=3.77\,\text{Å}$, $\sigma_{\mathrm{CH_2}}=3.93\,\text{Å}$, $\sigma_{\mathrm{CH}}=4.1\,\text{Å}$, $\epsilon_{\mathrm{CH_3}}/k_B=98.1\,\mathrm{K}$, $\epsilon_{\mathrm{CH_2}}/k_B=47\,\mathrm{K}$ and $\epsilon_{\mathrm{CH}}/k_B=12\,\mathrm{K}$). We have performed a simulation of squalane ($T=372\,\mathrm{K}$, $\dot{\gamma}=1.063\times10^9\,\mathrm{s}^{-1}$) using this latter LJ parameterization. Compared to the parameterization due to Mondello and Grest at the same strain rate ($R_g^2=48.7\,\text{Å}^2$, $P=-31.5$ MPa, $\nu=3.6\times10^{-6}\,\mathrm{m^2/s}$), this LJ parameterization for squalane yielded a somewhat smaller R_g^2 and significantly different pressure and kinematic viscosity ($R_g^2=45.5\,\text{Å}^2$, $P=37.2$ MPa, $\nu=2.3\times10^{-6}\,\mathrm{m^2/s}$). Thus, it seems probable that the success of Mondello and Grest's parameterization for squalane is due to their use of the large methyl energy parameter from SKS (for normal alkanes, $\epsilon_{\mathrm{CH_3}}/k_B=114\,\mathrm{K}$) as the energy parameter for the many methyl branches of squalane. Use of either of the smaller methyl energy parameters from parameterizations for branched alkanes ($\epsilon_{\mathrm{CH_3}}/k_B(\text{methyl branch})=78\,\mathrm{K}$ or $\epsilon_{\mathrm{CH_3}}/k_B=98.1\,\mathrm{K}$) evidently leads to viscosity predictions in poorer agreement with experiment for squalane itself but which are more consistent with the performance of the model for other linear and branched alkanes. This is consistent with the observation of Lahtela *et al.*[38] that small changes in the intermolecular potential parameters of the branched methyl group in 3-methylhexane produced large changes in viscosity. Martin and Siepmann have recently revised their united atom model for branched alkanes[39] and Chen and Siepmann have reported parameters for an explicit united atom model for normal alkanes.[40]

C. Chain configurations and shear-induced alignment

Molecular configurations and alignment in these alkane systems show significant strain-rate dependence at the high rates of shear covered in this study. The squared radius of gyration as a function of $\dot{\gamma}$ divided by its average value for $\dot{\gamma}<\tau_1^{-1}$ is plotted in Fig. 4. We chose to normalize by the low-$\dot{\gamma}$ values rather than the equilibrium ones because otherwise we would have to rely on the EMD results of Mondello and Grest which yielded R_g^2 values for squalane some-

what smaller than the low-$\dot{\gamma}$ values determined from our simulations. Previously,[33] Cui *et al.* attributed the small difference between their low-$\dot{\gamma}$ R_g^2 for *n*-decane and the EMD value of Mondello and Grest to the slightly increased flexibility of the model due to the bond vibrational potential used by Cui *et al.* and in the present work. Consistent with the conclusions of previous NEMD studies of alkanes,[12,22,33,41,42] R_g^2 for the linear alkane shows a maximum at intermediate strain rates. As was also observed by Khare *et al.* for 5,12-dipropylhexadecane,[12] R_g^2 for 9-*n*-octyldocosane does not show a maximum as a function of $\dot{\gamma}$. Squalane, with its many short side-branches, shows a slight maximum in R_g^2, behavior intermediate between that of the long, linear alkane and the long-branched alkane. Padilla and Toxvaerd[42] rationalized the occurrence of a maximum in R_g^2 as a competition between two mechanisms to relieve chain tension due to chains traversing multiple shear planes in the shear field: alignment of the chains with the flow field (the dominant mechanism at the lower strain rates) and deformation of the chain (the dominant mechanism at the higher strain rates). In each case in Fig. 4, the average chain dimension decreases with increasing $\dot{\gamma}$ at high $\dot{\gamma}$. Since the presence of branches would inherently hinder the ability to minimize a chain's exposure to multiple shear planes, it may not be surprising that the variation of R_g^2 with $\dot{\gamma}$ is less dramatic for the branched alkanes. In all cases the variation is fairly modest: at most a 10% increase or decrease.

One measure of the structural order in the system is the order tensor, defined as[43,44]

$$S=\frac{3}{2}\left\langle \frac{1}{N}\sum_{i=1}^{N}\left(e_i e_i-\frac{1}{3}l\right)\right\rangle, \tag{5}$$

where e_i is the unit vector along the end-to-end direction of the molecule *i*, *l* is a second-rank tensor with a value of 0 for the off-diagonal elements and a value of 1 for the diagonal elements, and the summation is over all *N* molecules in the system. The angle braces indicate an ensemble average. The eigenvector corresponding to the largest eigenvalue (the order parameter) of the order tensor gives the preferential orientation of the molecules relative to the flow field. This alignment angle is plotted versus strain rate in Fig. 5. Clearly, shear thinning in these systems is accompanied by the alignment of molecules with the flow direction. At low $\dot{\gamma}$, the alignment angle increases with decreasing $\dot{\gamma}$ as it approaches linear-regime behavior. At high $\dot{\gamma}$, it approaches a small limiting value between 6 and 11°. Cui *et al.*[15] associated the sharp decrease in the alignment angle with the transition from Newtonian to shear-thinning behavior and observed that the limiting value of the angle at high $\dot{\gamma}$ is dependent on the length of the molecule's backbone. This observation is confirmed here for the $C_{30}H_{62}$ isomers; as the chain-backbone length increased from 9-*n*-octyldocosane to squalane to *n*-triacontane, the limiting alignment angle decreased from approximately 10.5 to 7.7 to 6.8°. This trend illustrates the need of the longer molecules to better align with the flow field in order to dissipate the viscous force among them. The limiting high-$\dot{\gamma}$ value of the alignment angle is seen here to vary only slightly with temperature for the same molecule; for both 9-*n*-octyldocosane and squalane, the angle at 372 K is only slightly larger than the value at 311 K.

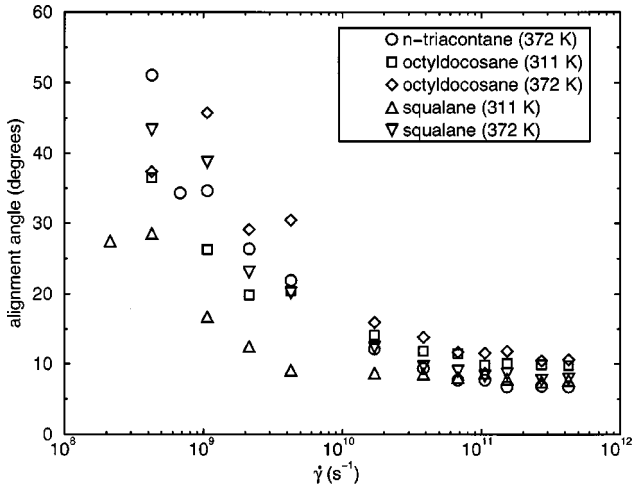

FIG. 5. The alignment angle with the flow field of the end-to-end vector for *n* triacontane and of the backbone of 9-*n*-octyldocosane and squalane.

D. Energies and hydrostatic pressure

At low strain rate, in most cases, the average energies vary over a fairly wide range. In contrast, at high strain rates the curves exhibit a certain amount of convergence; the bond-stretching+intramolecular-LJ energies and bond-angle-bending energies are segregated according to temperature while the torsional and intermolecular-LJ are segregated according to molecular identity. In Fig. 6, the hydrostatic pressure is plotted versus strain rate. Shear dilatancy is seen at high rates of shear in all cases with $P \propto \dot{\gamma}^p$ where *p* is equal to 0.57 (*n*-triacontane, 372 K), 0.52 (9-*n*-octyldocosane, 311 K), 0.54 (9-*n*-octyldocosane, 372 K), 1.15 (squalane, 311 K), and 1.53 (squalane, 372 K). Such a variety in the shear dilatancy is consistent with previous simulation studies that have yielded a diversity of results for alkanes.[19,22,33,41,45] Though not particularly obvious in Fig. 6, the hydrostatic

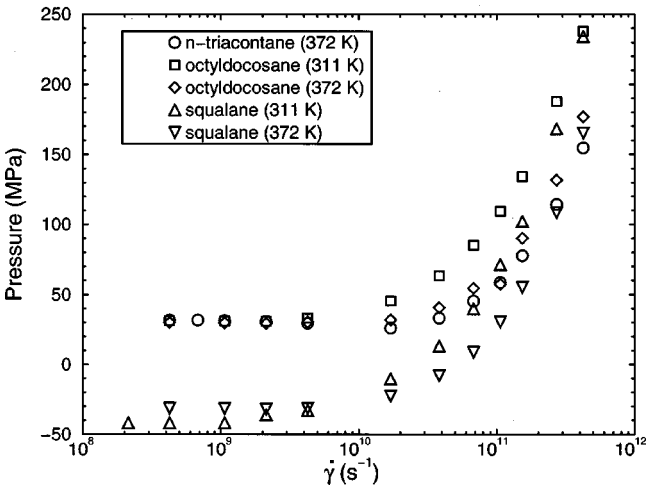

FIG. 6. Hydrostatic pressure as a function of $\dot{\gamma}$ for *n*-triacontane, 9-*n*-octyldocosane, and squalane.

pressure of *n*-triacontane passes through a minimum at $\dot{\gamma} = 1.70 \times 10^{10}\,s^{-1}$. A minimum in the average intermolecular-LJ energy per molecule is also observed at this strain rate. Khare *et al.* observed similar behavior for *n*-octacosane[12] as we also have for $n\text{-}C_{100}H_{202}$.[46] This can be understood in terms of two competing phenomena: the ordering induced by the shear field (tending to lower the energy) and the effect of the high rates of shear that cause more frequent and stronger collisions and keep chains out of the minimum energy states. The former effect dominates at lower strain rates and the latter at higher strain rates, leading to the occurrence of minima in the pressure and energy as a function of strain rate. These minima seem to occur at or just prior to the strain rate corresponding to the maximum in R_g^2 and are only observed for the normal alkanes.

III. CONCLUSIONS

We have reported EMD and NEMD simulations of *n*-triacontane, 9-*n*-octyldocosane, and squalane at temperatures of 311 and 372 K using a united atom model. Though no experimental diffusion data were available with which to compare the results for 9-*n*-octyldocosane, the model overpredicted the self-diffusion coefficient of *n*-triacontane at 372 K by 61%. Using the rotational relaxation time calculated from the EMD simulation and results from the Rouse model, the predicted zero-shear viscosity for *n*-triacontane was within 16% of the value determined by NEMD. Compared to experiment, NEMD and the united atom model underpredicted the kinematic viscosities of *n*-triacontane and 9-*n*-octyldocosane but accurately predicted the values for squalane (within 15%). In addition, the predicted VI values for both 9-*n*-octyldocosane and squalane were in quantitative agreement with experiment and represent the first such predictions by molecular simulation. That is, even though the united atom model did not accurately predict the viscosities for 9-*n*-octyldocosane, it still did an excellent job of predicting the dependence of its viscosity on temperature. Thus, this same general potential model and computational approach can be used to predict this important lubricant property for potential lubricants prior to their synthesis, offering the possibility of simulation-guided lubricant design. In terms of the properties examined in this study, 9-*n*-octyldocosane would be the best lubricant candidate among these two branched C_{30} isomers because it has the higher viscosity index (weaker variation of viscosity on temperature). For the $C_{30}H_{62}$ isomers, as the chain-backbone length increased the limiting alignment angle at high strain rate decreased. In addition, the high-$\dot{\gamma}$ value of the alignment angle varied only slightly with temperature for the same molecule. For the normal alkane only, a minimum was observed in the average hydrostatic pressure and intermolecular LJ potential energy at the strain rate just prior to the occurrence of the maximum in R_g^2.

ACKNOWLEDGMENTS

The majority of this computational research was performed on the Intel Paragons at the Center for Computational Sciences at Oak Ridge National Laboratory. Additional calculations were performed on Cray T3E supercomputers located at Cray Research in Eagan, Minnesota, and at the National Energy Research Scientific Computing Center at Lawrence Berkeley National Laboratory. This work was supported in part by a National Science Foundation Graduate Fellowship awarded to one of the authors (J.D.M.), the Chemical and Thermal Systems Program of the National Science Foundation, and the Division of Materials Sciences of the U.S. Department of Energy. Oak Ridge National Laboratory is operated for the Department of Energy by Lockheed Martin Energy Research Corp. under Contract No. DE-AC05-96OR22464.

[1] P. M. Morse, Chem. Eng. News **76**, 21 (1998).
[2] A. P. I., API 42: *Properties of Hydrocarbons of High Molecular Weight* (American Petroleum Institute, 1966).
[3] V. Eychenne and Z. Mouloungui, Ind. Eng. Chem. Res. **37**, 4835 (1998).
[4] J. Denis, J. Synth. Lub. **1**, 201 (1984).
[5] J. I. Siepmann, S. Karaborni, and B. Smit, Nature (London) **365**, 330 (1993).
[6] M. E. Tuckerman, B. J. Berne, and G. J. Martyna, J. Chem. Phys. **97**, 1990 (1992).
[7] S. Chynoweth, U. C. Klomp, and L. E. Scales, Comput. Phys. Commun. **62**, 297 (1991).
[8] R. A. Gray, S. Chynoweth, Y. Michopoulos, and G. S. Pawley, Europhys. Lett. **43**, 491 (1998).
[9] D. J. Evans and G. P. Morriss, *Statistical Mechanics of Nonequilibrium Liquids* (Academic, New York, 1990).
[10] S. S. Sarman, D. J. Evans, and P. T. Cummings, Phys. Rep. **305**, 1 (1998).
[11] C. J. Mundy, S. Balasubramanian, K. Bagchi, J. I. Siepmann, and M. L. Klein, Faraday Trans. **104**, 17 (1996).
[12] R. Khare, J. de Pablo, and A. Yethiraj, J. Chem. Phys. **107**, 6956 (1997).
[13] J. D. Moore, S. T. Cui, P. T. Cummings, and H. D. Cochran, AIChE J. **43**, 3260 (1997).
[14] M. Lahtela, M. Linnolahti, T. A. Pakkanen, and R. L. Rowley, J. Chem. Phys. **108**, 2626 (1998).
[15] S. T. Cui, P. T. Cummings, H. D. Cochran, J. D. Moore, and S. A. Gupta, Int. J. Thermophys. **19**, 449 (1998).
[16] S. A. Gupta, P. T. Cummings, and H. D. Cochran, J. Chem. Phys. **107**, 10316 (1997); **107**, 10327 (1997); **107**, 10335 (1997).
[17] M. Mondello and G. S. Grest, J. Chem. Phys. **103**, 7156 (1995).
[18] C. J. Mundy, J. I. Siepmann, and M. L. Klein, J. Chem. Phys. **102**, 3376 (1995).
[19] S. T. Cui, P. T. Cummings, and H. D. Cochran, J. Chem. Phys. **104**, 225 (1996).
[20] K. P. Travis and D. J. Evans, Mol. Simul. **17**, 157 (1996).
[21] K. P. Travis, P. J. Daivis, and D. J. Evans, J. Chem. Phys. **103**, 10638 (1995).
[22] A. Berker, S. Chynoweth, U. C. Klomp, and Y. Michopoulos, J. Chem. Soc., Faraday Trans. **88**, 1719 (1992).
[23] P. E. Rouse, Jr., J. Chem. Phys. **21**, 1272 (1953).
[24] M. Mondello, G. S. Grest, E. B. Webb, III, and P. Peczak, J. Chem. Phys. **109**, 798 (1998).
[25] T. Vardag, N. Krager, and H.-D. Lüdemann, Ber. Bunsenges. Phys. Chem. **95**, 859 (1991).
[26] P. Padilla and S. Toxvaerd, J. Chem. Phys. **94**, 5650 (1991).
[27] P. Padilla and S. Toxvaerd, J. Chem. Phys. **95**, 509 (1991).
[28] W. Paul, D. Y. Yoon, and G. D. Smith, J. Chem. Phys. **103**, 1702 (1995).
[29] P. Debye, *Polar Molecules* (Dover, New York, 1929).
[30] B. Berne and R. Pecora, *Dynamic Light Scattering* (Wiley, New York, 1976).
[31] H. Takeuchi and R.-J. Roe, J. Chem. Phys. **94**, 7446 (1991).
[32] M. Mondello and G. S. Grest, J. Chem. Phys. **106**, 9327 (1997).
[33] S. T. Cui, S. A. Gupta, and P. T. Cummings, J. Chem. Phys. **105**, 1214 (1996).
[34] W. Gleissle, Rheol. Acta **21**, 484 (1982).
[35] W.-M. Kulicke and R. Kniewske, Rheol. Acta **23**, 75 (1984).
[36] W. Allen and R. L. Rowley, J. Chem. Phys. **106**, 10273 (1997).
[37] J. I. Siepmann, M. G. Martin, C. J. Mundy, and M. L. Klein, Mol. Phys. **90**, 687 (1997).

[38] M. Lahtela, T. A. Pakkanen, and R. L. Rowley, J. Phys. Chem. A **101**, 3449 (1997).
[39] M. G. Martin and J. I. Siepmann, J. Phys. Chem. B **103**, 4508 (1999).
[40] B. Chen and J. I. Siepmann, J. Phys. Chem. B **103**, 5370 (1999).
[41] G. P. Morriss, P. J. Daivis, and D. J. Evans, J. Chem. Phys. **94**, 7420 (1991).
[42] P. Padilla and S. Toxvaerd, J. Chem. Phys. **97**, 7687 (1992).
[43] Chandrasekhar, *Liquid Crystals* (Cambridge University Press, Cambridge, 1992).
[44] P. G. de Gennes and J. Prost, *The Physics of Liquid Crystals* (Clarendon, Oxford, 1993).
[45] J. H. R. Clarke and D. Brown, J. Chem. Phys. **86**, 1542 (1987).
[46] J. D. Moore, S. T. Cui, H. D. Cochran, and P. T. Cummings, J. Non-Newtonian Fluid Mech. **93**, 83 (2000).